Transportation Research Part C 98 (2019) 139–151

Contents lists available at ScienceDirect

Transportation Research Part C

journal homepage: www.elsevier.com/locate/trc

Characterization of bicycle following and overtaking maneuvers on cycling paths

Hossameldin Mohammed, Alexander Y. Bigazzi, Tarek Sayed*

Department of Civil Engineering, University of British Columbia, 6250 Applied Science Lane, Vancouver, BC V6T 1Z4, Canada

A B S T R A C T

A better understanding of cyclist behavior during various interactions is needed to enhance bicycle microsimulation models. This study aims to characterize cyclist maneuvers in following and overtaking interactions using multivariate finite mixture model-based clustering. Several variables that potentially affect cyclist state and future decisions are extracted from video data using computer vision techniques, including the longitudinal distance, lateral distance and speed difference between interacting cyclists. Observations of cyclists in following interactions are clustered into constrained and unconstrained states. Observations of overtaking cyclists are clustered into initiation, merging and post-overtaking states. Multivariate distributions within each cluster are examined, along with state transitions for each type of interaction. These characterizations are a key step toward development of agent-based bicycle traffic microsimulation models, which can be used to enhance bicycle facility planning and design, safety modeling, and energy modeling.

1. Introduction

Active modes of transportation such as cycling are promoted as a way to provide health benefits, mitigate traffic congestion and reduce air pollution (Götschi et al., 2016). As such, there is significant interest in research to develop cycling behavior models to enhance the design and evaluation of investments in bicycle infrastructure (Heinen et al., 2010). Better understanding of how cyclists move and interact is essential for developing bicycle microsimulation models, which can be used in traffic modeling, safety evaluation, energy and health modeling, and more.

Advances in motor vehicle traffic simulation models can guide the development of bicycle traffic simulation models. Since the 1960s, many car-following and lane-change models have been developed for motor vehicle traffic simulation. Car-following models can be generally classified into three main types (Aghabayk et al., 2015): stimulus response models such as the General Motors (GM) model (Chandler et al., 1958) & (Gazis et al., 1961), safe distance models such as the Gipps model (Gipps, 1981), and action point models such as the Wiedemann model (Leutzbach and Wiedemann, 1986). Most of these models follow a general framework of first identifying the state or the regime a vehicle is in by acquiring perceptual variables such as speeds and positions of that vehicle and its adjacent interacting vehicles (Aghabayk et al., 2015), (Ahmed and Ben-Akiva, 1996). For example, VISSIM (PTV, 2011) utilizes an action point model by identifying different regimes for each vehicle in each time step, i.e. free driving, approaching, following, and braking regime (Fellendorf and Vortisch, 2001). For each regime, VISSIM predicts a vehicle's acceleration or deceleration in the next time step based on speed, speed difference, distance and individual characteristics of driver and vehicle. A vehicle can transition from one regime to another if it exceeds a certain threshold described as a combination of speed difference and distance. Another example is AIMSUN (AIMSUN User's Manual, 2005), which utilizes a safe distance model. A vehicle in AIMSUN can be in a free-flow or constrained regime. Different rules are applied to vehicles in each state to predict acceleration in the next time step (Rakha and Wang, 2009). Lane change models follow a similar approach to car-following models by modeling the lane change process as a series of

* Corresponding author.
E-mail addresses: hos40044@mail.ubc.ca (H. Mohammed), abigazzi@civil.ubc.ca (A.Y. Bigazzi), tsayed@civil.ubc.ca (T. Sayed).

https://doi.org/10.1016/j.trc.2018.11.012
Received 16 July 2018; Received in revised form 14 November 2018; Accepted 23 November 2018
Available online 30 November 2018
0968-090X/

decisions, such as the decision to initiate a lane change and the target lane (Ahmed, 1999).

Cycling behavior and bicycle maneuvers in traffic are different from those of motor vehicles, due to distinct physical and dynamic characteristics (Twaddle et al., 2014). Bicycle traffic flow is often non-lane based and cyclists more freely utilize lateral road space (Taylor and Mahmassani, 1998). Bicycle traffic is also characterized by high heterogeneity in behavior and performance among cyclists (Hoogendoorn and Daamen, 2016). Some commercial traffic microsimulation software such as VISSIM, PARAMICS and AIMSUN provide the option to simulate bicycle traffic using modified variations of motor vehicle microsimulation models. The performance of these models has not been sufficiently validated (Carrignon, 2009; COWI, 2012).

Few studies have investigated states or regimes in bicycle traffic. Liang et al. developed a social force model that describes bicycle traffic as either free-flow or congested flow regimes (Liang et al., 2012). Ma and Luo (2016) used bicycle GPS data to identify cruising, acceleration and deceleration regimes; interactions were not examined. Zhao and Zhang (2017) used an experiment of bicycles on a circular track to develop a model for bicycle following and a unified following model for motor vehicle, bicycle and pedestrian flow, but the model was not validated with on-road data. Hoogendoorn and Daamen (2016) developed distributions of following bicycle headways and segmented into constrained and unconstrained headways. Khan and Raksuntorn (2001) studied bicycle overtaking maneuvers on separated bicycle facilities by comparing speeds of overtaking bicycles at different overtaking states. Zhao et al. (2013) developed and calibrated a cellular automata model for modeling overtaking decisions of mixed bicycle traffic consisting of conventional and electric bicycles. The developed model was used to predict the number of the overtaking events at different bicycle traffic densities. Further research is needed to characterize cyclist states in various types of interactions and develop representative bicycle traffic microsimulation models in a variety of contexts.

The objective of this research is to characterize cyclist states in following and overtaking interactions by examining multivariate distributions from clustered observations of on-road cyclists. The scope of investigation includes unidirectional cyclists on dedicated bicycle paths. A Gaussian Finite Mixture Model (GFMM) is used to cluster the perceptual variables of longitudinal distances, lateral distances and speed differences between interacting cyclists. The characterization of cyclist interactions and the identification of the distributions of variables in each state is an important step toward the development of agent-based microscopic simulation models, which consider individual cyclists as autonomous agents who take actions bounded by behavioral rules (Jennings, 2000).

The main intended application of the presented research is the development of bicycle microsimulation models. Agent-based microsimulation models require rules for agents in distinct traffic situations to predict decisions such as acceleration, change in longitudinal and lateral positions, etc. For example, the rules applied for cyclist agents in free flow state will be different from rules applied in constrained or overtaking states. The determination of thresholds of perceptual variables between states is an essential step in bicycle microsimulation. Determination of cyclist states is also important for prediction of cyclist behavior in different situations, which is essential in safety evaluation, particularly for shared-space infrastructure and connected vehicle technology.

2. Methodology

2.1. Data

Video data were collected at the Brooklyn Bridge, New York City, USA (Fig. 1). Two cameras were mounted on fixed objects of the bridge to capture two scenes on September 20, 2016. For each scene two hours of video were recorded from 8:00 to 9:00 and from 17:00 to 18:00 at a frame frequency of 15 Hz. The bridge carries motor vehicle, pedestrian and bicycle traffic in both directions. The pedestrian-bicycle path is four meters wide, divided by pavement marking into two equal-width lanes, one for bidirectional bicycle traffic and the other for bidirectional pedestrian traffic. The two path sections captured in the video scenes have two-meter bicycle lanes and two-meter pedestrian lanes. The path has a 1% upgrade in one direction and 1% downgrade in the other direction at the two studied sections.

Bicycle trajectories were extracted from the videos using automated computer vision techniques developed at the University of British Columbia. A detailed description of the video analysis procedure can be found in Saunier and Sayed (2006). The system was used in the collection of microscopic cyclist data (Zaki and Sayed, 2016; Zaki et al., 2013). The first step of the video analysis is camera calibration, which relates the two-dimensional video data with real-world three-dimensional coordinates (Ismail et al., 2008). Camera calibration involves determining the location and orientation of the camera, and then estimating a homography matrix which represents the projection parameters between the video data and real-world space.

Moving features in the video data were differentiated from background fixed features and tracked using the Kanade-Lucas-Tomasi Feature Tracker (Lucas and Kanade, 1981; Tomasi and Kanade, 1994). The tracked features were then grouped based on parameters of vision cues such as spatial proximity and typical size of tracked objects (Fig. 2). The computer vision detection accuracy decreases with the increase in depth of the trajectory. All the trajectories were truncated at a length of 65 m to account for the decrease in location detection accuracy with the increase in depth. That truncation length was determined by observing higher projection plane distortion after this distance. Counts of the detected bicycles and pedestrians in the four hours of video data are shown in Table 1. Pedestrian trajectories were excluded from further analysis as few interactions with cyclists were observed due to the separation of bicycle and pedestrian lanes on the paths.

The extracted trajectories are composed of a local longitude and latitude for each cyclist at each video frame, relative to a predetermined origin point on the world map of the camera scene view. The spatiotemporal trajectories were used to calculate speed for each cyclist at each video frame by first calculating an instantaneous speed (distance divided by time) and then applying a Savitzky–Golay filter (Savitzky and Golay, 1964) with a seven time-step (7/15 s) window size. A validation of the trajectory extraction process was conducted by taking a sample of 30 trajectories from each hour of video (sample of 120 trajectories) and

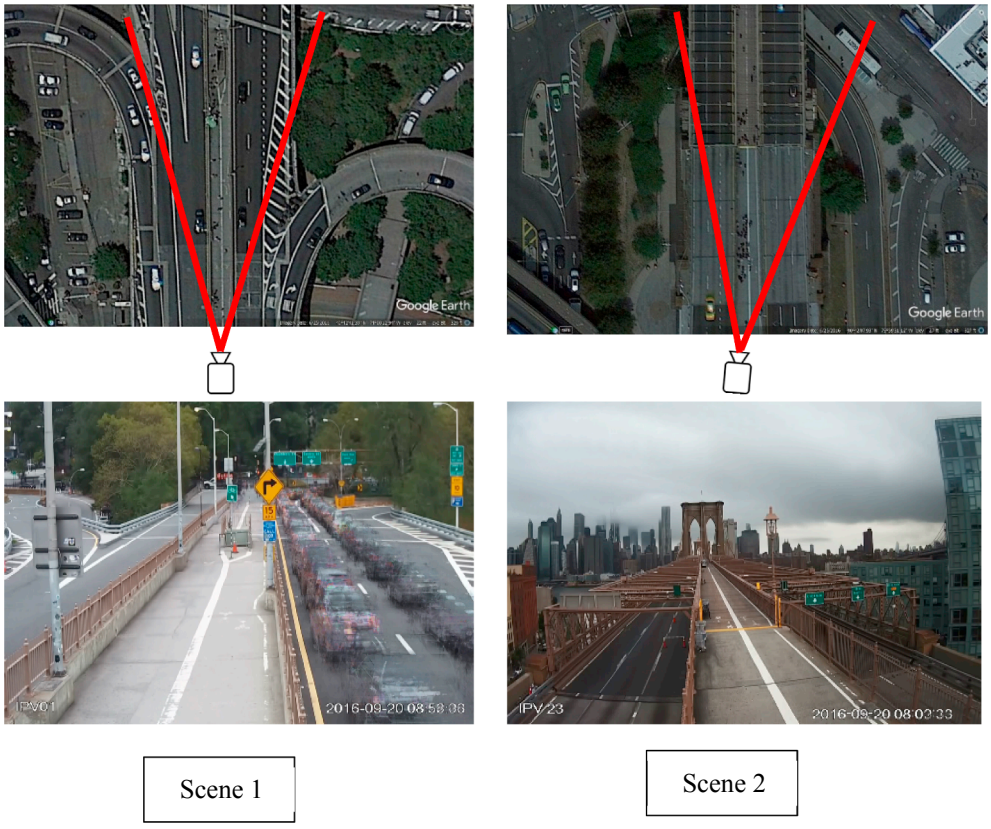

Fig. 1. Camera positions and field of view of the two video scenes.

Fig. 2. Feature detection and object grouping visualization.

Table 1
Bicycle and pedestrian volume counts.

	Scene 1 Sept. 20, 2016 8:00–9:00	Scene 1 Sept. 20, 2016 17:00–18:00	Scene 2 Sept. 20, 2016 8:00–9:00	Scene 2 Sept. 20, 2016 17:00–18:00	Total
Bicycle Volume	421	223	349	131	1124
Pedestrian Volume	365	976	336	1333	3010

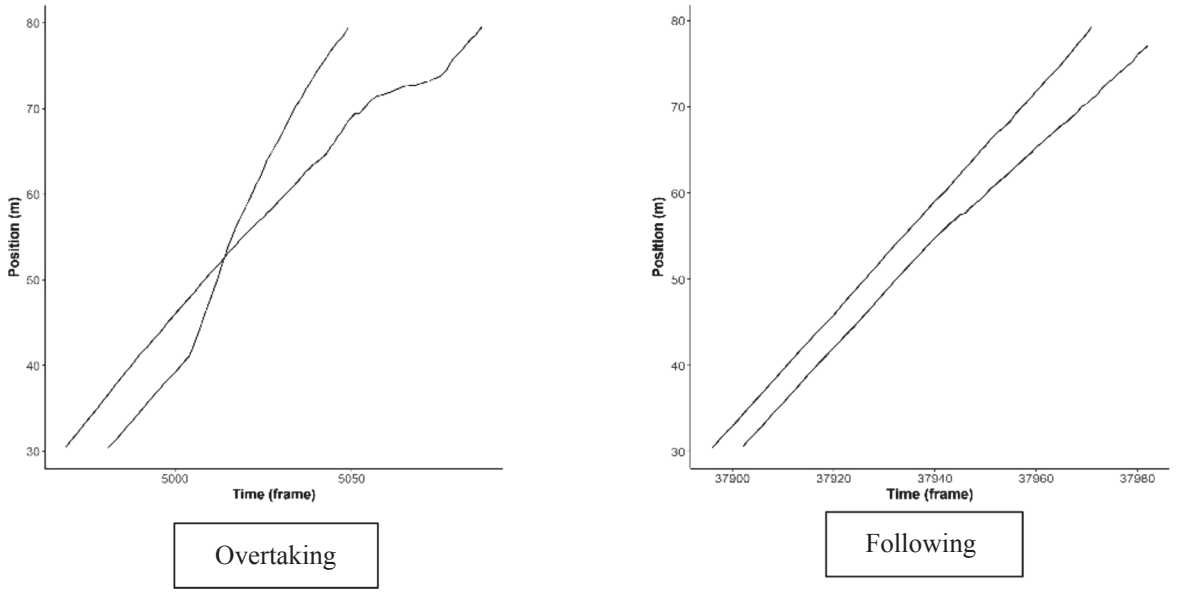

Fig. 3. Example trajectories in overtaking and following interactions.

manually measuring the speed based on the time required to traverse a known distance in the video scene. The mean absolute error between automatically extracted speed and manually-measured speed was 0.86 m/s, which was considered negligible to not affect the findings. Almost 95% of the cyclists' trajectories were detected using the computer vision technique with an average trajectory duration of 5 s.

2.2. Interactions

Bicycle trajectories in a single direction that co-existed in any frame of data were considered to be in potential following or overtaking interactions. The minimum observed time headway between non-interacting cyclists was 10 s, which is considered sufficient to treat them as not being involved in an interaction. If three or more trajectories co-existed in a single frame of data, separate interactions were identified between sequential pairs of cyclists. The average duration of interacting trajectories was 3 s with 1.5 s standard deviation. Overtaking interactions were differentiated from following interactions by plotting space-time diagrams to identify overtaking events where the trajectories crossed (Fig. 3), and then visually confirming by watching the relevant video data. The data were captured over four highly directional hours, in which the two morning hours (8:00–9:00) had approximately 90% of the traffic in the direction going to Manhattan, and the other two hours (17:00–18:00) had approximately 70% of the traffic in the direction going to Brooklyn. The extracted following and overtaking interactions were rarely concurrent with the presence of counter-flowing traffic, which was consistent with the study scope of unidirectional interactions. Any trajectories with interactions with counter-flowing traffic were excluded from the analysis data. Out of 1124 identified bicycle trajectories, 590 were involved in 316 following interactions (some cyclists were involved in two following interactions simultaneously as leader in one interaction and a follower in the other), and 68 were involved in 34 overtaking interactions (half overtaking and half being overtaken) – see Fig. 4.

Three perceptual variables were calculated from the trajectories in each interaction, based on previous cycling behavior research (Liang et al., 2012; Hoogendoorn and Daamen, 2016; Zhao, et al., 2013): longitudinal distance, lateral distance, and speed difference. The longitudinal distance is the distance along the path between the tracking points of two interacting cyclists, negative when the

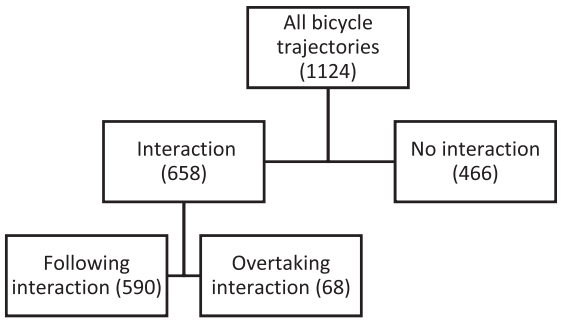

Fig. 4. Classification of bicycle trajectories by interactions (number of trajectories).

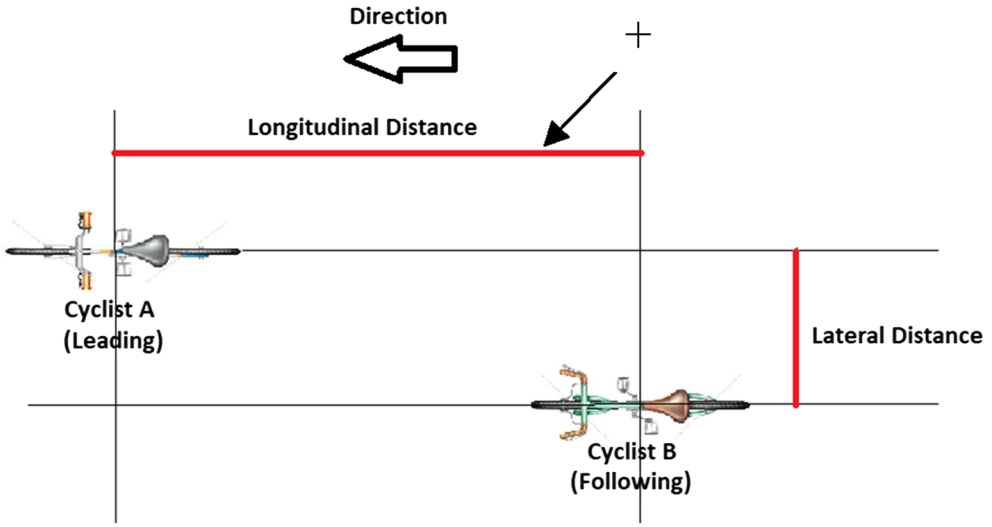

Fig. 5. Longitudinal and lateral distance between two interacting cyclists.

initially leading cyclist is ahead (as illustrated in Fig. 5). The lateral distance is the absolute distance perpendicular to the path between the tracking points of two interacting cyclists (Fig. 5). The speed difference is that of the initially following cyclist minus that of the initially leading cyclist (i.e., positive when the initially following cyclist is faster).

2.3. State identification

The characterization of states of bicycle maneuvers during interactions was conducted by classifying the disaggregate measured perceptual variables (longitudinal distance, lateral distance, and speed difference) into homogeneous subgroups within each interaction. Gaussian Finite Mixture Model (GFMM) was selected as the clustering method because it does not require an assumption of spherical variable distributions within the clusters (Everitt and Hand, 1981). GFMM attempts to recover the model of data generation assuming the data population consists of multiple subpopulations in which the variables have different multivariate joint Gaussian probability density functions. The resulting distributions can vary in features such as size, orientation, and shape, which allows for flexibility in fitting the models (Banfield and Raftery, 1993).

The twelve shape criteria based on re-parameterization of the cluster covariance matrices given in Banfield and Raftery (1993) were evaluated using the Bayesian Information Criteria (BIC). The shape model "VVV" (Varying size, Varying shape, and Varying orientation with ellipsoidal covariance) was selected based on lowest BIC for both interaction types. The cluster model was estimated using the *MCLUST* package in the statistical software R (Scrucca et al., 2016).

The GFMM clustering method assumes the input observations of the model are independent and identically distributed (IID). The pooled trajectory data used in the GFMM clustering contains repeated measurements of cyclist variables, which leads to potential serial dependence. One approach to model this dependency is to add a random effect coefficient to the finite mixtures of linear mixed models (Celeux et al., 2005). However, previous research found no significant difference between the clustering results obtained with and without random effect coefficients (Pelosi et al., 2015). The autocorrelation coefficient was calculated for every variable in the data and the coefficient value had an average value of 0.32 which is considered low. Also, the Durbin-Watson statistic was calculated for the first order autoregressive process, and the value of the statistic was 1.6, which indicates no evidence of autocorrelation under 95% confidence level (Gujarati, 2003). The low autocorrelation coefficient could be due to the large number of individual cyclists in the data which decreases the effect of serial dependence (Guo et al., 2013). As no strong serial dependence was concluded from the data, it was decided not to model the serial dependence in the cluster analysis.

Following interactions represented by the perceptual variables of 316 pairs of cyclist trajectories were clustered into two states of motion, hypothesized to represent constrained and unconstrained flow states based on past research (Hoogendoorn and Daamen, 2016; Buckley, 1968). The overtaking interactions represented by the perceptual variables 34 pairs of cyclist trajectories were clustered into three states of motion, hypothesized to represent initiation, merging, and post-overtaking phases based on past research that examined the relationships between speeds, longitudinal distance and lateral distance in overtaking maneuvers (Khan and Raksuntorn, 2001). Although these three states were not explicitly concluded in Khan and Raksuntorn (2001), the three-cluster hypothesis was proposed in light of the patterns discovered by exploratory analysis of the relationships between the three motion variables conducted in the paper. Fig. 6 illustrates the three hypothesized phases of an overtaking interaction. Absolute speed difference was used in clustering following interactions and speed difference was used in clustering overtaking interactions.

Intuitively, there is likely a preceding fourth state of the overtaking cyclist just before the initiation state, but an exploratory analysis of the dataset indicated no such fourth cluster in the data. For example, the longitudinal distance has a low frequency of large negative values (only 2% of the values more than -20 m), indicating that most of the captured overtaking maneuvers began in the

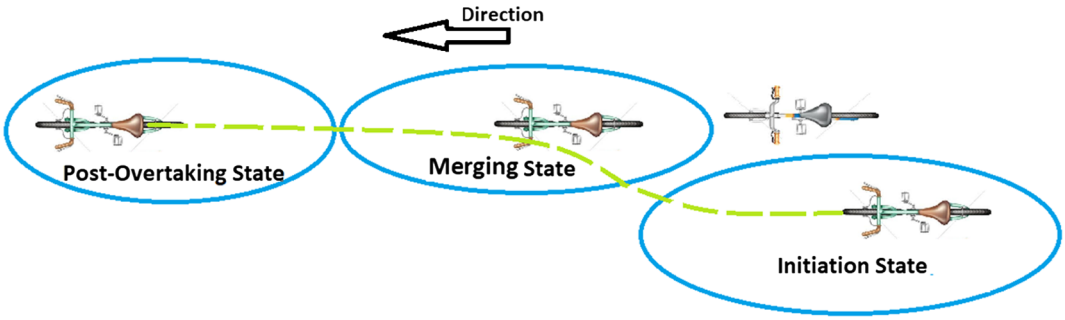

Fig. 6. The hypothesized initiation, merging and post-overtaking phases of an overtaking interaction – blue ovals indicate the overtaking cyclist. (For interpretation of the references to colour in this figure legend, the reader is referred to the web version of this article.)

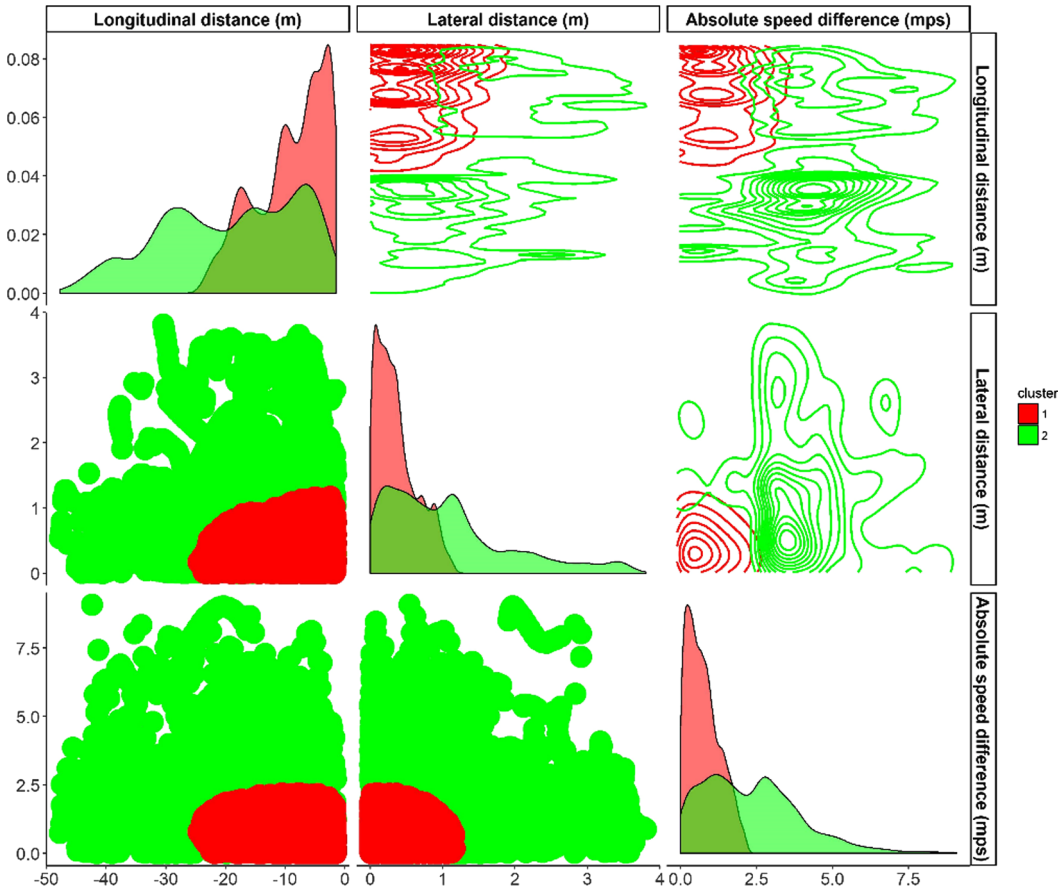

Fig. 7. Density distributions (diagonal), cluster scatterplots (below the diagonal) and density plots (above the diagonal) for following interaction clustering results.

initiation state. One reason why the data do not include a "pre-overtaking" state is the duration of the captured trajectories, which limit the observation of both a pre-overtaking and post-overtaking state in the same trajectory pair. That reasoning is supported when comparing the BIC values of different numbers of clusters, as the BIC value is lower for three clusters than four clusters.

Bootstrapping was used to evaluate the uncertainty in the mixing densities and cluster distributions. The GFMM clustering method was applied individually to 1000 resamples of 90% of the original dataset, to obtain distributions of model parameters. In addition, to check the consistency of the results, the oscillation between different states or clusters within an interaction was evaluated.

2.4. State thresholds identification

The states obtained from clustering analysis were used as input to a supervised classification problem to identify the structure and decision boundaries of perceptual variables between clusters. Decision Trees model (Breiman et al., 1983) was selected for the

Table 2
Summary of perceptual variables by cluster in following interactions.

	Cluster 1				Cluster 2			
Number of observations	5117				4584			
	Mean	Standard deviation	Range		Mean	Standard deviation	Range	
			Min.	Max.			Min.	Max.
Longitudinal distance (m)	−9.27	5.97	−24.56	−1.51	−18.71	10.89	−47.75	−1.51
Lateral distance (m)	0.37	0.28	0	1.17	0.98	0.82	0	3.81
Absolute speed difference (m/s)	0.77	0.57	0	2.19	2.22	1.55	0	9.08

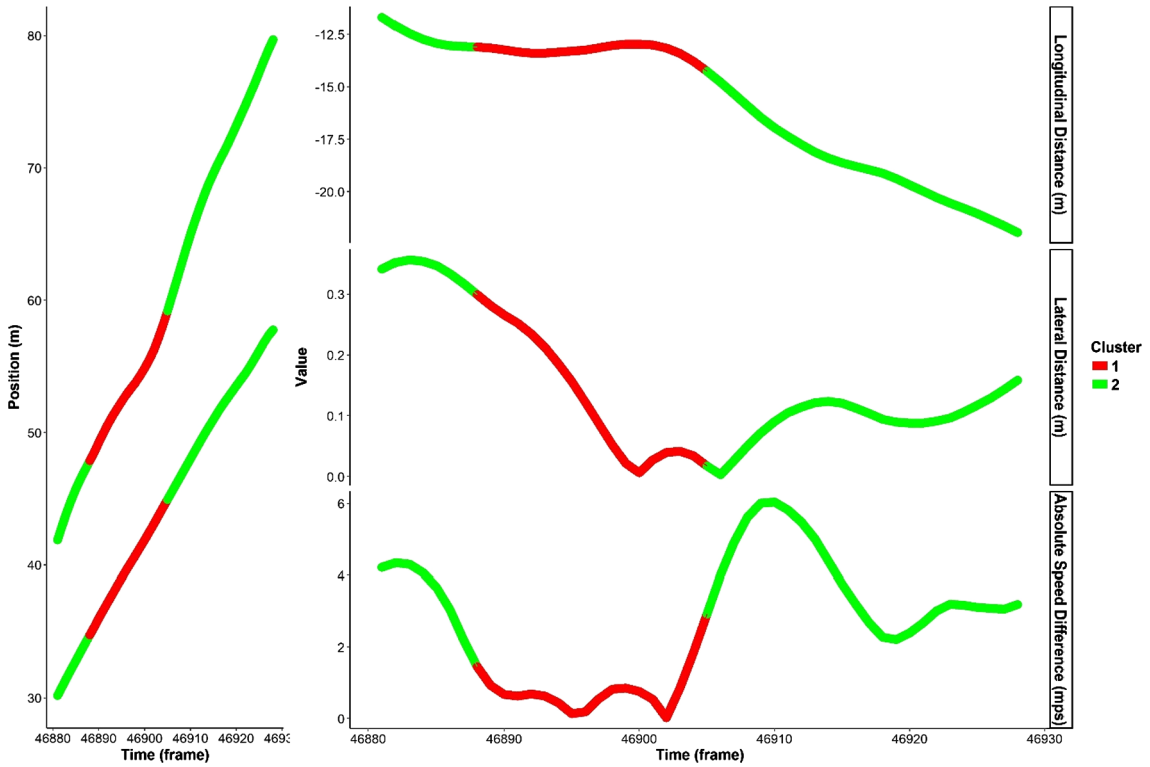

Fig. 8. Example trajectories in a following interaction with clustering results.

classification. The tree is built by first finding the variable that best splits the data into two groups. The splitting process is applied recursively to each sub-group, until the size of the tree reaches a maximum desired value and/or the number of points in subgroups reaches a minimum value. The recursive splitting was done according to information criteria, which splits every parent node by selecting the threshold that divides the data into the child nodes that have the purest classes. The decision trees model was estimated using the *RPART* package in the statistical software R (Therneau and Atkinson, 2018). The classification algorithm first divides the data into 10 randomly selected samples. For each sample a decision tree is grown and a risk parameter for misclassification is calculated by comparing the model predicted classes and the true classes. A complexity parameter which gives the lowest risk is calculated. All the data are finally used to fit the model using the calculated complexity parameter.

3. Results

The clustering results for following interactions are presented in Fig. 7 and Table 2. Clusters were assigned for 10,422 single-frame observations within the 316 following interactions, roughly evenly split between the two clusters. Cluster 1 has longitudinal distances of −25 to −1.5 m, lateral distances of 0–1.2 m, and absolute speed differences of 0–2.2 m/s. Cluster 2 has wider ranges of all three variables: longitudinal distances with a minimum of -48 m, lateral distances up to 3.8 m, and speed differences up to 9.1 m/s. The values of very high speed difference (9 m/s) were investigated by inspection of the video data, revealing interactions in which the following cyclist in an unconstrained state slows to observe the scenery or due to some other distraction. Also the downgrade of 1% in

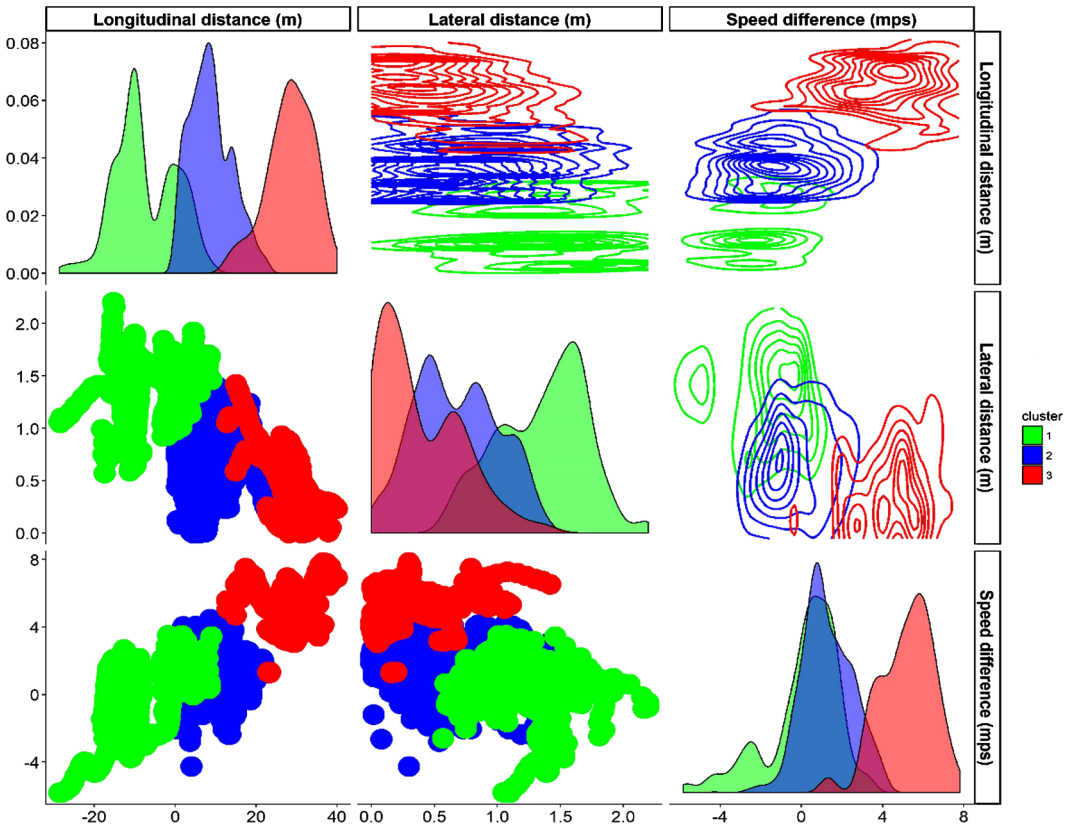

Fig. 9. Density distributions (diagonal), cluster scatterplots (below the diagonal) and density plots (above the diagonal) for overtaking interaction clustering results.

Table 3
Summary of perceptual variables by cluster in overtaking interactions.

	Cluster 1				Cluster 2				Cluster 3			
Number of observations	630				1457				213			
	Mean	SD	Range		Mean	SD	Range		Mean	SD	Range	
			Min.	Max.			Min.	Max.			Min.	Max.
Longitudinal distance (m)	−5.12	7.84	−28.61	8.96	8.07	5.45	0.4	22.95	28.09	5.69	12.81	39.97
Lateral distance (m)	1.51	0.82	0.57	2.20	0.70	0.33	0	1.39	0.37	0.30	0	1.42
Speed difference (m)	0.92	1.93	−5.83	3.51	1.18	1.31	−4.27	4.45	4.82	1.64	1.26	7.82

one direction is another cause of observing very high speeds. Cluster 2 also has higher absolute means and larger standard deviations than cluster 1 for all three variables.

The more narrow distributions of perceptual variables in cluster 1 suggest that it represents a constrained state in a following interaction. In this state, the following cyclists have closely matched the lateral position and speed of the leading cyclist, and are in relatively close longitudinal proximity. The univariate distributions of the clustering variables in cluster 2 are wide and include low values of all three variables, but not simultaneously. A following cyclist is unconstrained (i.e. in cluster 2) with a high value of longitudinal distance, lateral distance, or speed difference, even if the other two values are low.

An example is given in Fig. 8 of a pair of trajectories in a following interaction with clustering results. The following cyclist transitions from an unconstrained to a constrained state as the speed difference falls, and then returns to an unconstrained state as the speed difference increases again and the longitudinal distance increases as a result. The lateral distance is small throughout the interaction.

The clustering results for overtaking interactions are presented in Fig. 9 and Table 3. Clusters were assigned for 2300 single-frame observations within the 34 overtaking interactions. Clusters 1, 2, and 3 have increasing longitudinal distances, with mean values of -5, 8, and 28 m respectively. Lateral distances are highest for cluster 1 (mean of 1.5 m), and lower for the other two clusters (means of

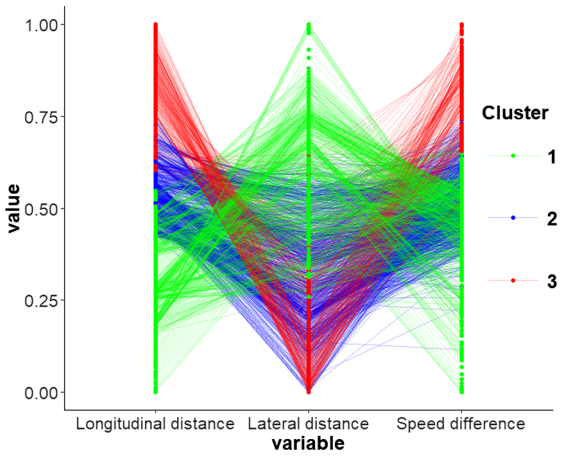

Fig. 10. Multivariate relationships among clustering variables in overtaking interactions.

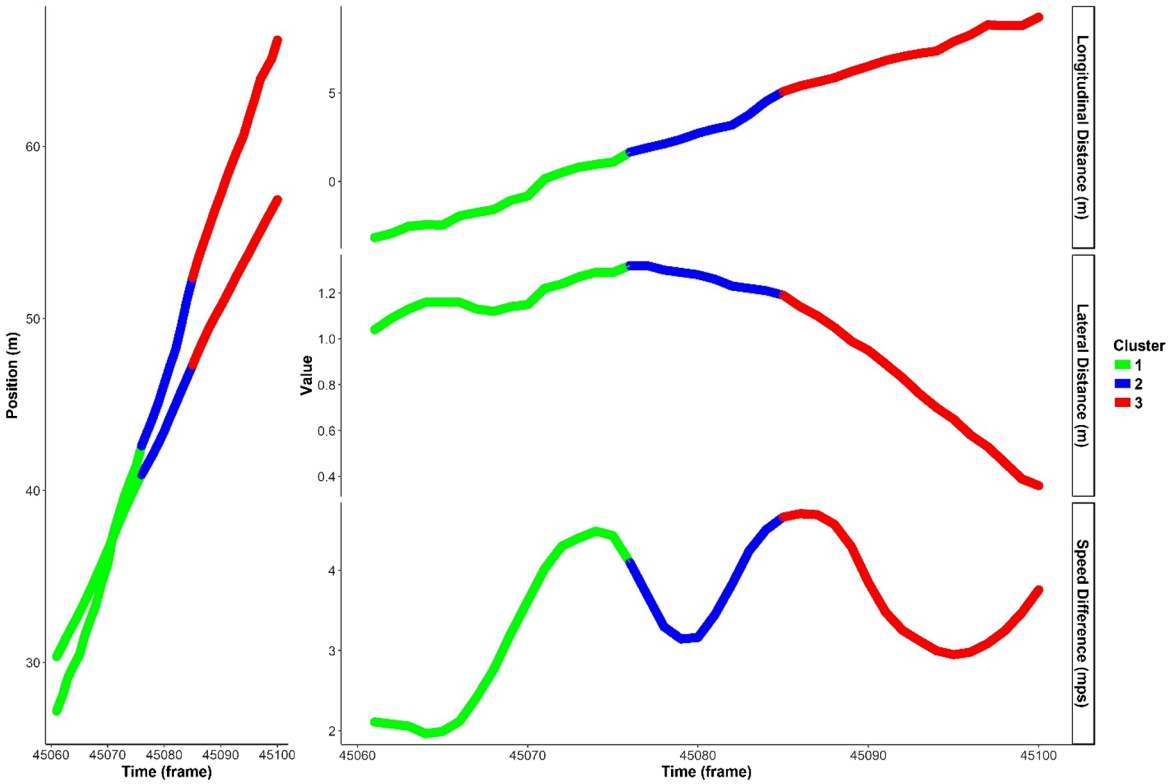

Fig. 11. Example trajectories in an overtaking interaction with clustering results.

0.3 and 0.4 for clusters 2 and 3, respectively). The speed difference is lowest in clusters 1 and 2 (means of 1 m/s), and higher cluster 3 (mean of 5 m/s).

The variable values in the three clusters are consistent with the three hypothesized phases of an overtaking interaction illustrated in Fig. 6. Cluster 1 can be interpreted as the initiation state, in which the overtaking cyclist initiates the maneuver from an initially negative longitudinal distance, with a positive speed difference and high lateral distance. Cluster 2 is characterized by positive but low values of longitudinal distance, lower values of lateral distances and similar speed difference, which is indicative of the merging state in which the overtaking cyclist has passed and is attempting to return to a non-interacting path. Cluster 3 can be interpreted as the post-overtaking state, in which the overtaking cyclist is far ahead of the other cyclist and has achieved their desired, higher speed, which is reflected in large positive values of longitudinal distance and speed difference, and low lateral distance.

The parallel coordinates plot given Fig. 10 connects the three relative variable values (scaled to the variable ranges) for each observation, colored by cluster. Observations in cluster 1 have high lateral distance but low longitudinal distance and speed

Table 4
Bootstrapping results of following and overtaking clustering.

			Longitudinal distance (m)	Lateral distance (m)	Speed difference (m/s)
Following	Cluster 1	Mean	9.13	0.37	0.76
		SD	0.15	0.01	0.01
		Range of means	(8.73; 9.72)	(0.34; 0.38)	(0.71; 0.81)
	Cluster 2	Mean	18.63	0.97	2.2
		SD	0.15	0.01	0.02
		Range	(18.1; 19.1)	(0.94; 1)	(2.13; 2.27)
Overtaking	Cluster 1	Mean	−5.06	1.34	0.86
		SD	0.41	0.02	0.08
		Range of means	(−5.47; −4.61)	(1.28; 1.39)	(−0.08; 1.1)
	Cluster 2	Mean	7.17	0.55	0.95
		SD	0.22	0.01	0.04
		Range	(6.88; 8.73)	(0.52; 0.72)	(0.83; 1.21)
	Cluster 3	Mean	27.94	0.4	4.98
		SD	0.49	0.02	0.23
		Range of means	(24.89; 29.39)	(0.32; 0.49)	(3.61; 5.48)

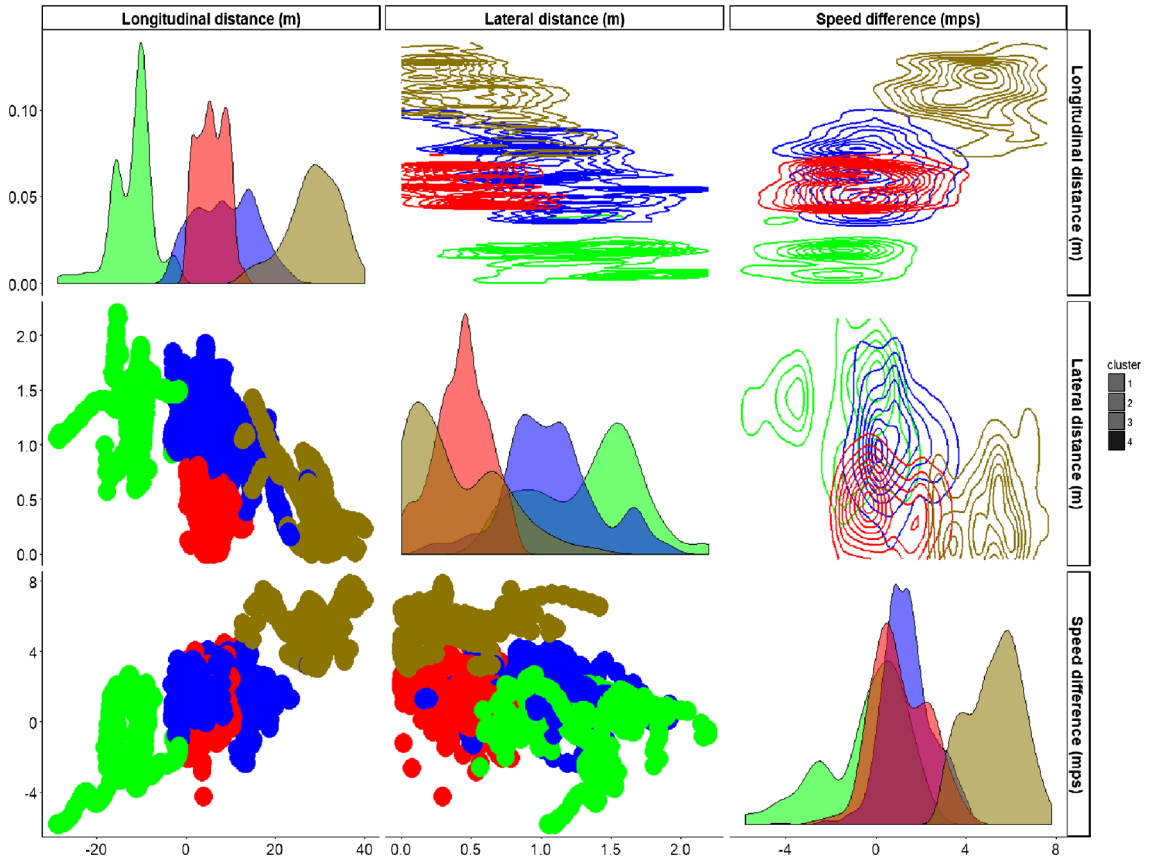

Fig. 12. Density distributions (diagonal) and cluster scatterplots (off-diagonal) for overtaking interaction clustering results.

difference, whereas cluster 3 is the opposite and cluster 2 is a transition between them.

Fig. 11 gives an example of a pair of trajectories in an overtaking interaction with clustering results. The overtaking cyclist begins in an initiation state, then transitions to a merging state and finally to a post-overtaking state, consistent with the proposed labels for clusters 1, 2, and 3. The longitudinal distance increases throughout, and the lateral distance falls after completing the maneuver. The speed difference increases during the initiation state, then fluctuates, but is consistently high throughout.

Table 4 gives the results of the bootstrapping analysis for following and overtaking interactions, respectively. The distribution of variable means within clusters is low, indicating that the clustering algorithm is robust. The maximum coefficient of variation is 0.09.

Most following interactions (57%) had zero transitions between clusters, partially due to the short duration of some of the observed interactions, while 14% had 1 transition, 14% had 2 transitions, and 15% had 3 or more transitions (maximum of 6). Most

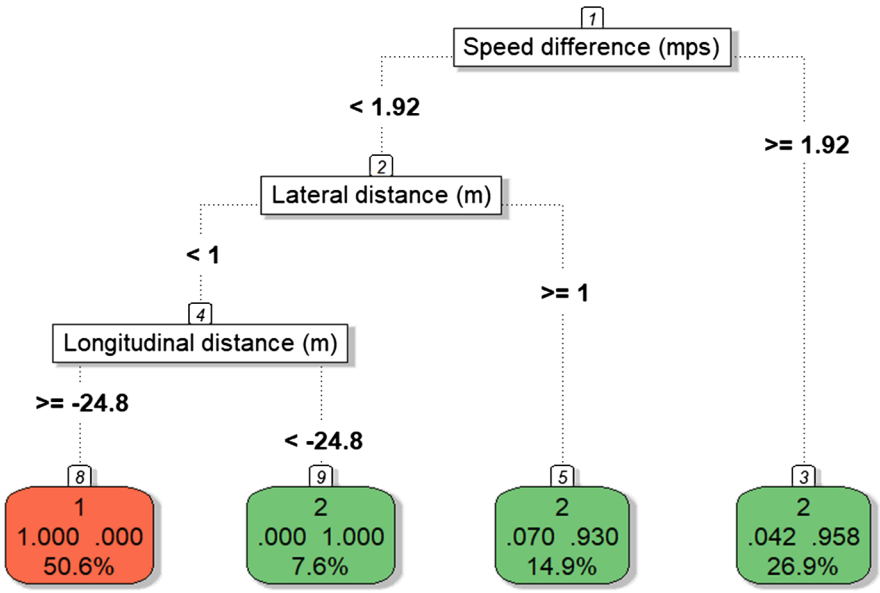

Fig. 13. Structure and thresholds of variables in following interaction states (each final class box shows the cluster number, fraction of points correctly classified, fraction of points mis-classified, and % of total observations).

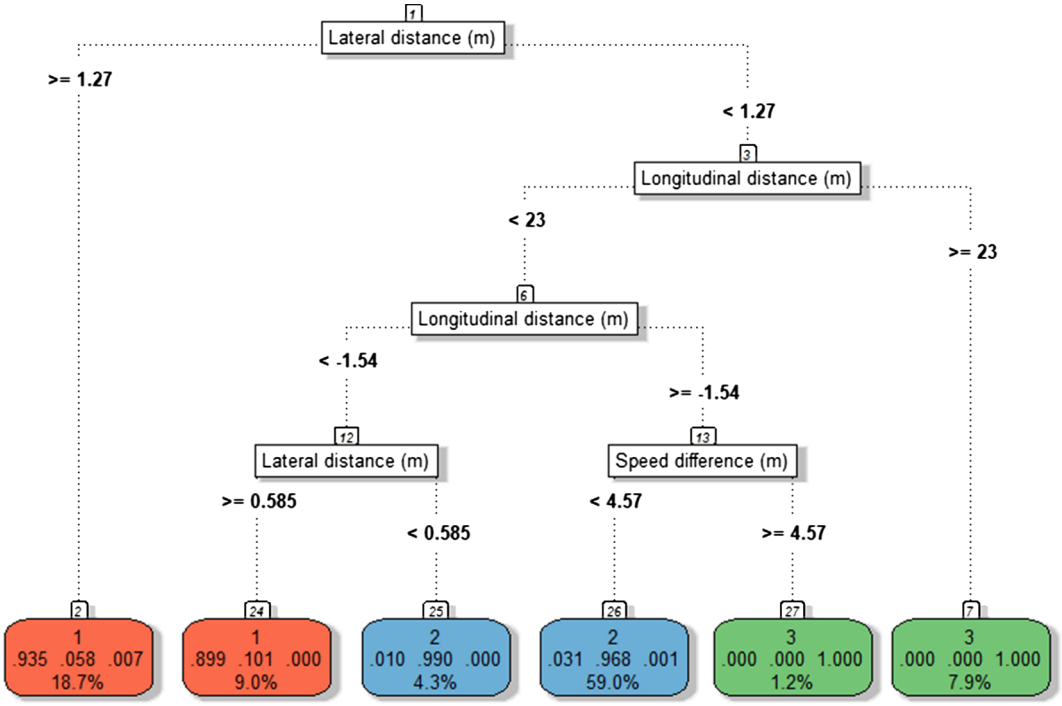

Fig. 14. Structure and thresholds of variables in overtaking interaction states (each final class box shows the cluster number, fraction of points correctly classified, fraction of points mis-classified, and % of total observations).

overtaking interactions (67%) had exactly 2 transitions between clusters, while 8% had 3 transitions, and 25% had 4 or more transitions (again a maximum of 6). No overtaking interactions had fewer than 2 transitions, and all overtaking interactions included all three clusters. The sequential stability of the clusters (i.e., little oscillation between clusters within an interaction), supports the robustness of the clustering approach for characterizing bicycling states of motion.

An analysis of overtaking clusters was conducted assuming four clusters to compare to the three clusters results (Fig. 12). The results do not have an intuitive explanation, as the first cluster has a similar distribution as the clustering analysis using three clusters (Fig. 9), but the second and third clusters are not significantly different in longitudinal distance values, which are centered around

Table 5
Confusion matrix of following and overtaking classification results.

Following Confusion Matrix			
		Predicted cluster	
		"1"	"2"
True Class	"1"	51%	0%
	"2"	2%	47%

Overtaking Confusion Matrix				
		Predicted Cluster		
		"1"	"2"	"3"
True Class	"1"	25%	1%	0%
	"2"	2%	62%	0%
	"3"	0%	0%	9%

zero. The only significant difference between the second and third clusters is the lateral distance, which does not indicate the addition of a pre-initiation state with the fourth cluster, but rather a second merging state with two different passing distances. It can be concluded from the results that the analysis using three clusters is more suitable to the data, which is in most cases lacking the pre-initiation state in which a cyclist takes the decision to overtake.

The structure and thresholds of variables were identified by applying the decision tree model to the results of clustering analysis of the following and overtaking interactions. The results of the following interactions decision tree model are shown in Fig. 13. The following data are initially split by the absolute speed difference at a threshold of 1.9 m/s. Data points that exceed 1.9 m/s absolute speed difference are classified into the unconstrained state (cluster 2). The remaining data are split again at a lateral distance threshold of 1 m, and then a longitudinal distance threshold of 25 m. Thus, data points are classified into the constrained state (cluster 1) if they have an absolute speed difference below 1.9 m/s, lateral distance below 1 m, and longitudinal distance less than 25 m; otherwise, they are classified as unconstrained (cluster 2).

The classification tree of overtaking states is shown in Fig. 14. First the data points are split at a lateral distance threshold of 1.3 m. Lateral distances of 1.3 m or more are classified as the initiation state (cluster 1). The other data points are split again at a longitudinal distance threshold of 23 m, for which longer distances are classified as the post-overtaking state (cluster 3). The next split is at a longitudinal distance threshold of −1.5 m (nearly parallel cyclists), after which observations below that threshold are split into initiation and merging states at a lateral distance of 0.58. Observations above the −1.5 m longitudinal distance threshold are split into merging and post-overtaking states at a speed difference 4.6 m/s.

The confusion matrices for the following and overtaking data classifications are given in Table 5. The confusion matrix is a representation of the relationship between the true and predicted classes by the model. The table shows a low misclassification error rate of 2% and 3% in following and overtaking trees, respectively.

4. Discussion and conclusion

The results of this study indicate that the threshold of longitudinal distance between constrained and unconstrained states in following interactions is 25 m, which equates to a 5 s time headway at 5 m/s average speed. This finding is supported by Hoogendoorn and Daamen (2016), in which the threshold between constrained and unconstrained cycling was estimated to be 4 s. In our study, the constrained longitudinal distance ranges from 1.5 m to 24 m with an average of 9 m; the minimum longitudinal distance is supported by the value measured in Zhao and Zhang (2017) of 2.0. The threshold of lateral distance between constrained and unconstrained states is 1 m, slightly higher than the value set in Hoogendoorn and Daamen (2016) of 0.7 m, based on the width of cyclist handlebars plus an additional shy-away distance. In overtaking interactions, the average speed difference in initiation state is 1.2 m/s, which is lower than the values measured in Khan and Raksuntorn (2001) and Falkenberg et al. (2003) of 2.6 and 3.6 m/s, respectively. In addition to using different samples, those two studies used subjective methods to determine the initiation stage of the overtaking interaction.

The sample size used in the analysis of overtaking interaction of 34 overtaking interactions with 2300 observation can be argued to be small. However, there is no clear standard in the literature for calculating the minimum sample size for clustering analysis. The minimum sample size should be correlated with the dimensionality of the problem (Dolnicar, 2002). Past studies provide methods for assessing the sample size in clustering analysis, such as (Formann, 1984), which mentions a rule to assess the number of clusters according to the number of variables used in the clustering as the minimum number of observations to be ($5 * 2^m$), where m is the number of variables. According to this rule, the sample size used in this study is considered sufficient. In any study, more conclusive results could be obtained using a larger sample size.

There are several limitations to this study. First, the method used for clustering needs to be tested with other datasets from different contexts such as different facility types, road grades and cities. Second, the trajectories extracted from the video data were short in duration, so some interactions could have started in the field of vision of the video scenes and completed out of it. Third, there are only two locations in the video data. Validation of the variable distributions and thresholds in different states is required to

test the applicability and transferability to other locations. Fourth, other types of interactions such as between bi-directional cyclists and between cyclists and pedestrians should also be investigated. Fifth, cyclist behavior in groups was not considered in following interactions. More research in cyclists' group following behavior can reveal further behavioral characteristics. Finally, trajectories could not be extracted from the video data for 100% of cyclists, which might have biased the sample if the tracking failures were non-random.

Future research can apply the distributions and thresholds of variables in different states to develop interaction rules specific to each state. These rules can describe the predicted change in acceleration and direction in each time step based on the perceptual variables. Other variables such as accelerations and yaw rates could also be tested for inclusion in clustering. Modeling other types of interactions will also be required for the development of improved bicycle microsimulation models. Finally, using other datasets containing trajectories longer in duration can help capturing the full overtaking maneuvers including the decision to initiate the overtaking.

References

Aghabayk, K., Sarvi, M., William, Y., 2015. A state-of-the-art review of car-following models with particular considerations of heavy vehicles. Transp. Rev. 1 (35), 82–105.

Ahmed, K.I., 1999. Modeling Drivers' Acceleration and Lane Changing Behavior. Institute of Technology, Massachusetts.

Ahmed, K.I., Ben-Akiva, M., 1996. Models of freeway lane changing and gap acceptance behavior. Transport. Traffic Theory 13, 501–515.

AIMSUN User's Manual, 2005. TSS-Transport Simulation System.

Banfield, J.D., Raftery, A.E., 1993. Model-based Gaussian and non-Gaussian clustering. Biometrics 49 (3), 803–821.

Breiman, L., Friedman, J.H., Olshen, R.A., Stone, C.J., 1983. Classification and Regression Trees. Wadsworth, Belmont, California.

Buckley, D.J., 1968. A semi-poisson model of traffic flow. Transport. Sci. 2 (2), 107–132.

Carrignon, D., 2009. Assessment of the impact of cyclists on heterogeneous traffic. TEC Magaz. 323–325.

Celeux, G., Martin, O., Lavergne, C., 2005. Mixture of linear mixed models for clustering gene expression profiles from repeated microarray experiments. Stat. Model. 5 (3), 243–267.

Chandler, R.E., Herman, R., Montroll, E.W., 1958. Traffic dynamics: studies in car following. Oper. Res. 6 (2), 165–184.

COWI, 2012. Micro Simulation of Cyclists in Peak Hour Traffc. Copenhagen.

Dolnicar, S., 2002. A review of unquestioned standards in using cluster analysis for data-driven market segmentation. Australian and New Zealand marketing academy conference (ANZMAC). Melbourne.

Everitt, B.S., Hand, D.J., 1981. Finite Mixture Distributions. Chapman and Hall CRC, London.

Falkenberg, G., Blasi, A., Bonfranchi, T., Cosse, L., Draeger, W., Vortisch, P., Zimmermann, A., 2003. Bemessung von Radverkehrsanlagen unter verkehrstechnischen Gesichtspunkten. Unterreihe Verkehrstechnik.

Fellendorf, M., Vortisch, P., 2001. Validation of the microscopic traffic flow model VISSIM in different real-world situations. In: Transportation Research Board 80th annual meeting. Washington, D.C.

Formann, A.K., 1984. Die Latent-Class-Analyse: Einführung in Theorie und Anwendung. Beltz, Weinheim.

Gazis, D., Herman, R., Rothery, R.W., 1961. Nonlinear follow-the-leader models of traffic flow. Oper. Res. 9 (4), 545–567.

Gipps, P.G., 1981. A behavioral car-following model for computer simulation. Transport. Res. Part B: Methodol. 15 (2), 105–111.

Götschi, T., Garrard, J., Giles-Corti, B., 2016. Cycling as a part of daily life: a review of health perspectives. Transp. Rev. 36 (1), 45–71.

Gujarati, D.N., 2003. Basic Econometrics. Mc-Graw Hill.

Guo, Y., Logan, H.L., Glueck, D.H., Muller, K.E., 2013. Selecting a sample size for studies with repeated measures. BMC Med. Res. Method. 13 (1).

Heinen, E., Bert, V., Kees, M., 2010. Commuting by bicycle: an overview of the literature. Transp. Rev. 30 (1), 59–96.

Hoogendoorn, S., Daamen, W., 2016. Bicycle headway modeling and its applications. Transp. Res. Rec.: J. Transport. Res. Board 2587, 34–40.

Ismail, K., Sayed, T., Saunier, N., 2008. A methodology for precise camera calibration for data collection applications in urban traffic scenes. Can. J. Civ. Eng. 40 (1), 96–104.

Jennings, N., 2000. On agent-based software engineering. Artif. Intell. 117 (2), 277–296.

Khan, S., Raksuntorn, W., 2001. Characteristics of passing and meeting maneuvers on exclusive bicycle paths. Transport. Res. Rec.: J. Transport. Res. Board 1776, 220–228.

Leutzbach, W., Wiedemann, R., 1986. Development and applications of traffic simulation models at the Karlsruhe Institut fur Verkehrwesen. Traffic Eng. Control 27 (5).

Liang, X., Baohua, M.A., Qi, X.U., 2012. Psychological-physical force model for bicycle dynamics. J. Transport. Syst. Eng. Inform. Technol. 12 (2), 91–97.

Lucas, B.D., Kanade, T., 1981. An Iterative Image Registration Technique with an Application to Stereo Vision. In: International Joint Conference on Artificial Intelligence, pp. 674–679.

Ma, X., Luo, D., 2016. Modeling cyclist acceleration process for bicycle traffic simulation using naturalistic data. Transport. Res. Part F: Traffic Psychol. Behav. 40, 130–144.

Pelosi, M., Alfò, M., Martella, F., Pappalardo, E., Musarò, A., 2015. Finite mixture clustering of human tissues with different levels of IGF-1 splice variants mRNA transcripts. BMC Bioinf. 16 (1).

PTV, 2011. VISSIM 5.40 user manual. Karlsruhe, Germany.

Rakha, H., Wang, W., 2009. Procedure for calibrating Gipps car-following model. Transport. Res. Rec.: J. Transport. Res. Board 2124, 113–124.

Saunier, N., Sayed, T., 2006. A feature-based tracking algorithm for vehicles in intersections. In: Third Canadian Conference on Computer and Robot Vision. Quebec City, Quebec, Canada.

Savitzky, A., Golay, M.J., 1964. Smoothing and differentiation of data by simplified least squares procedure. Anal. Chem. 36 (8), 1627–1639.

Scrucca, L., Fop, M., Murphy, T.B., Raftery, A.E., 2016. mclust 5: clustering, classification and density estimation using Gaussian finite mixture models. R J. 8 (1), 2055–2233.

Taylor, D.B., Mahmassani, H.S., 1998. Behavioral Models and Characteristics of Bicycle-Automobile Mixed-Traffic: Planning and Engineering Implications. University of Texas, Austin.

Therneau, T., Atkinson, B., 2018. rpart: Recursive Partitioning and Regression Trees. R package version 4.1-13. Retrieved from < https://CRAN.R-project.org/package=rpart > .

Tomasi, C., Kanade, T., 1994. Detection and Tracking of Point Features. In: IEEE Conference on Computer Vision and Pattern Recognition, pp. 593–600.

Twaddle, H., Schendzielorz, T., Fakler, O., 2014. Bicycles in urban areas: review of existing methods for modeling behavior. Transport. Res. Rec.: J. Transport. Res. Board 2434, 140–146.

Zaki, M., Sayed, T., 2016. Automated cyclist data collection under high density conditions. IET Intel. Transport Syst. 10 (5), 361–369.

Zaki, M., Sayed, T., Cheung, A., 2013. Computer vision techniques for the automated collection of cyclist data. Transport. Res. Rec.: J. Transport. Res. Board 2387, 10–19.

Zhao, D., Wang, W., Li, C., Li, Z., Fu, P., Hu, X., 2013. Modeling of passing events in mixed bicycle traffic with cellular automata. Transport. Res. Rec.: J. Transport. Res. Board 2387, 26–34.

Zhao, Y., Zhang, H.M., 2017. A unified follow-the-leader model for vehicle, bicycle and pedestrian traffic. Transport. Res. Part B: Methodol. 105, 315–327.